A Pansharpening Algorithm Based on Morphological Filters

Rocco Restaino[1], Gemine Vivone[2], Mauro Dalla Mura[3(✉)], and Jocelyn Chanussot[3,4]

[1] Dept. of Information Eng., Electrical Eng. and Applied Math. (DIEM), University of Salerno, Fisciao, Italy
restaino@unisa.it

[2] North Atlantic Treaty Organization (NATO) Science and Technology Organization (STO) Centre for Maritime Research and Experimentation, La Spceizia, Italy
mauro.dalla-mura@gipsa-lab.grenoble-inp.fr

[3] GIPSA-lab, Grenoble-INP, Saint Martin d'Hères, France

[4] Faculty of Electrical and Computer Engineering, University of Iceland, Reykjavik, Iceland

Abstract. The fusion of multispectral and panchromatic images acquired by sensors mounted on satellite platforms represents a successful application of data fusion called *Pansharpening*. In this work we propose an algorithm based on morphological pyramid decomposition. This approach implements a Multi Resolution scheme based on morphological gradients for extracting spatial details from the panchromatic image, which are subsequently injected in the multispectral one. Several state-of-the-art methods are considered for comparison. Quantitative and qualitative results confirm the capability of the proposed technique to obtain pansharpened images that outperform state-of-the-art approaches.

Keywords: Mathematical Morphology · Pansharpening · Morphological filtering · Remote sensing · Image enhancement

1 Introduction

Pansharpening refers to a precise problem in data fusion that is the fusion of a MultiSpectral (MS) and a PANchromatic (PAN) image. The MS image is characterized by a high spectral resolution but a low spatial resolution whereas the PAN image has a greater spatial resolution but it acquires an unique spectral band. These images are acquired simultaneously by a PAN and MS sensors mounted on the same platform, as for satellites such as GeoEye and Worldview. The aim of pansharpening is the generation of a synthetic high spatial resolution MS image having the spatial features of the PAN image and the spectral resolution of the MS image. Several applications exploit data provided by pansharpening algorithms such as Google Earth and Microsoft Bing.

The pansharpening literature has been quickly growing in the last years, see [26] for a recent review. Pansharpening algorithms are often grouped into

J.A. Benediktsson et al. (Eds.): ISMM 2015, LNCS 9082, pp. 98–109, 2015.
DOI: 10.1007/978-3-319-18720-4_9

two families: The Component Substitution (CS) and the Multi-Resolution Analysis (MRA) methods. CS methods are based on the transformation of the MS image in another feature space (e.g., with a transformation in the Intensity-Hue-Saturation (IHS) representation [8] or with the Principal Component Analysis (PCA) [8]), where the spatial structure of the data can be more easily decoupled from the spectral information. The fusion process consists in the substitution of the component encompassing the spatial structure by the PAN image and in the subsequent reconstruction of the MS image. The MRA methods instead are based on the generation of a low resolution version of the PAN image for example using a multiresolution decomposition (i.e., a *pyramid*) of the image based on low-pass filters. Spatial details are then extracted from the PAN image as the residuals with respect to the low resolution PAN and injected, opportunely weighted, into the MS bands. The algorithm for constructing the low resolution PAN image and the injection coefficients (i.e., the weights applied to the spatial details) distinguish the different MRA methods.

In this paper we focus on this latter approach and in particular on the way the spatial details are extracted from the PAN. The largest majority of MRA techniques employs linear analysis operators ranging from to the wavelet/contourlet decompositions [20] to pyramids with Gaussian filters [2]. Another distinguishing feature among MRA approaches is the possible presence of decimation at each level of the decomposition that helps for compensating aliasing in the MS image [4]. A possible alternative for obtaining a pyramidal decomposition is offered by non-linear operators such as Morphological Filters (MF) [24]. Indeed some MFs are more effective than linear filters in preserving edges, allowing for superior perfomances in several applications, as, for example, geodesic reconstruction [21] and sharpening [17]. For that reason, morphological pyramids have also been used for fusing images with different characteristics in tasks such as the enhancement of optical imaging systems [6] and medical diagnostics [18]. Nevertheless, morphological pyramids have not received much attention in pansharpening. To the best of our knowledge, only the works of [13,14,1] address the pansharpening problem using approaches based on MFs, but a systematic study on their potentialities in this applicative domain has not been yet carried out. This has motivated us to explore this research direction by analyzing the effect of several different morphological analysis operators and structuring elements.

2 Pansharpening Based on MultiResolution Analysis

Let us denote by $\mathbf{MS}$ the available MS image, which is a three-dimensional array obtained by stacking N monochromatic images $\mathbf{MS}_k$ (i.e., the single spectral channels), with $k = 1, \ldots, N$, each composed by $n_r^{MS} \times n_c^{MS}$ pixels. Furthermore let us denote by $\mathbf{P}$ the available PAN image, composed by $n_r^{PAN} \times n_c^{PAN} = rn_r^{MS} \times rn_c^{MS}$ pixels. $r > 1$ is the ratio between the MS and PAN spatial resolution. The objective of the pansharpening process is to produce a synthetic MS image $\widehat{\mathbf{MS}}$ with the same spectral features of $\mathbf{MS}$ (i.e., N spectral bands) and with the same spatial resolution of $\mathbf{P}$ (i.e., $n_r^{PAN} \times n_c^{PAN}$).

Classical pansharpening algorithms follow the general scheme based on the injection of spatial details extracted from the PAN image to the MS bands [26]:

$$\widehat{\mathbf{MS}}_k = \widetilde{\mathbf{MS}}_k + g_k \mathbf{D}_k = \widetilde{\mathbf{MS}}_k + g_k \left(\mathbf{P} - \mathbf{P}_k^{low} \right), \tag{1}$$

in which $k = 1, \ldots, N$ specifies the spectral band, $\widetilde{\mathbf{MS}}_k$ and $\mathbf{D}_k$ are the k-th channels of the MS image upsampled to the PAN scale and of the injected details, respectively, and $\mathbf{g} = [g_1, \ldots, g_k, \ldots, g_N]$ are the *injection gains*. $\mathbf{P}_k^{low}$ denotes a low resolution version of the PAN image that, in general, may depend on the band k and it is obtained as a combination of the MS image spectral bands in CS methods and through a multiresolution decomposition within the MRA class.

In this paper we focus on the latter approach, in which a sequence of images with successively reduced resolution(also called approximations) is constructed through iterations, yielding the required image $\mathbf{P}_k^{low} = \mathbf{P}_k^L$, which is the image of the last level in the decomposition of $\mathbf{P}$ into L levels (i.e., the level of lowest resolution). Starting from the initial image $\mathbf{P}_k^0$ that is typically obtained by equalizing the PAN image $\mathbf{P}$ with respect to $\mathbf{MS}_k$, the decomposition proceeds with the recursion

$$\mathbf{P}_k^l = T_k^l \left[\mathbf{P}_k^{l-1} \right], \qquad l = 1, 2, \ldots L,$$

in which the *decomposition operators* $\left\{ T_k^l \right\}_{l=1,\ldots L}$ can be different, in principle, across the scales and the bands. In general for decimated pyramids, $T^l = R^{\downarrow} \psi_l$, so it comprises a filtering step, which is implemented by the generic *analysis operators* ψ_l, and downsampling with a rate R, denoted by $R^{\downarrow}$ (in general $R = 2$). Usually, the same filter is used across scales, i.e., $\psi_l = \psi$. For decimated decompositions it is necessary to expand the last level of the pyramid to the size of the PAN through an interpolation step $\mathrm{INT}^{\uparrow}$. In undecimated decompositions the spatial support of the decomposed image is not reduced at the different resolution levels, hence no downsampling is performed (i.e., $R = 1$) and no expansion is applied to the last level of the pyramid (i.e., $\mathrm{INT}^{\uparrow} = id$ with id the identity transform). However, the filtering operator ψ_l needs to vary with the levels for obtaining images with progressively reduced resolution. For linear pyramids the analysis operator is obtained through the convolution with a mask h_l, namely $\psi_l[\cdot] = h_l * \cdot$. Typical operators employed in pansharpening are average and Gaussian filters and wavelets [26].

Once the image $\mathbf{D}_k$ is computed, the details need to be injected to the MS bands. The strategies commonly employed rely on a multiplicative or additive injection scheme [26]. The former is referred to *High-Pass Modulation* (HPM) scheme in which the injection gains are given by:

$$g_k = \frac{\widetilde{\mathbf{MS}}_k}{\mathbf{P}_k^{low}}, \quad k = 1, \ldots, N. \tag{2}$$

The latter is called *High-Pass Filtering* (HPF) scheme and is implemented by setting $g_k = 1$.

3 Pansharpening Based on Morphological Filtering

This work is devoted to explore pansharpening algorithms based on morphological pyramidal decompositions. We briefly recall in the following the definition of some MFs and later, how they can be used for performing a decomposition in pansharpening.

3.1 Recall of Morphological Filters

In the following we will introduce the MFs considering a generic scalar image defined in a subset E of $\mathbb{Z}^2$ and with values in a finite subset V of $\mathbb{Z}$, i.e., $\mathbf{I} : E \subseteq \mathbb{Z}^2 \to V \subseteq \mathbb{Z}$. In this work we focus on MFs based on a set called *Structuring Element* (*SE*) B, that defines the spatial support in which the operator acts on the image [21]. We denote the spatial support of B as $N_B(\mathbf{x})$ that is the neighborhood with respect to the position $\mathbf{x} \in E$ in which B is centered. Flat SEs will be considered, so all elements in the neighborhood have unitary values and the only free parameters for defining B are the origin and N_B. We recall below the definition of the two basic operators of *Erosion* $\varepsilon_B(\mathbf{I})$ and *Dilation* $\delta_B(\mathbf{I})$:

$$\varepsilon_B(\mathbf{I})(\mathbf{x}) = \bigwedge_{\mathbf{y} \in N_B(\mathbf{x})} \mathbf{I}(\mathbf{y}); \quad \delta_B(\mathbf{I})(\mathbf{x}) = \bigvee_{\mathbf{y} \in N_B(\mathbf{x})} \mathbf{I}(\mathbf{y}). \tag{3}$$

Their sequential composition produces *Opening* and *Closing*, respectively defined as:

$$\gamma_B(\mathbf{I})(\mathbf{x}) = \delta_{\check{B}}[\varepsilon_B(\mathbf{I})(\mathbf{x})], \quad \phi_B(\mathbf{I})(\mathbf{x}) = \varepsilon_{\check{B}}[\delta_B(\mathbf{I})(\mathbf{x})], \tag{4}$$

with $\check{B}$ denoting the SE obtained by reflecting B with respect to its origin. The residual of the application of erosion is referred to as morphological *internal gradient* $\rho_B^-(\mathbf{I}) = \mathbf{I} - \varepsilon_B(\mathbf{I})$. Analogously, we have an *external gradient* considering a dilation: $\rho_B^+(\mathbf{I}) = \delta_B(\mathbf{I}) - \mathbf{I}$. In general, ρ^+ and ρ^- (named also *half-gradients*) are computed with a SE with smallest support. The operators extracting the residuals of opening and closing are referred to as top-hat transforms. Specifically, an opening defines a *White Top Hat*, $\mathrm{WTH}_B(\mathbf{I}) = \mathbf{I} - \gamma_B(\mathbf{I})$ and closing a *Black Top Hat*, $\mathrm{BTH}_B(\mathbf{I}) = \phi_B(\mathbf{I}) - \mathbf{I}$. The composition of erosion and dilation have proven useful for sharpening images through the so called *Toggle Contrast*, TC, mapping [21]:

$$\mathrm{TC}_B(\mathbf{I})(\mathbf{x}) = \begin{cases} \delta_B(\mathbf{I})(\mathbf{x}), & \text{if } \rho_B^+(\mathbf{I})(\mathbf{x}) < \rho_B^-(\mathbf{I})(\mathbf{x}), \\ \varepsilon_B(\mathbf{I})(\mathbf{x}), & \text{otherwise.} \end{cases} \tag{5}$$

3.2 Morphological Pyramids for Pansharpening

The composition of elementary morphological operators leads to the design of nonlinear pyramidal schemes [10,11,22]. Morphological decomposition approaches date back to Toet *et al.* [23], in which the multiscale representation

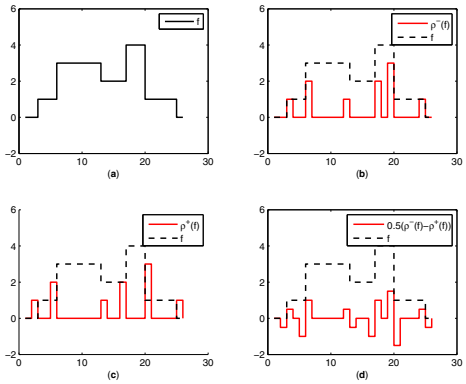

Fig. 1. Examples of morphological gradients, obtained through a flat SE with $N_B = \{-1, 0, 1\}$: (a) function f, (b) internal gradient $\rho^- = f - \epsilon_B(f)$; (c) external gradient $\rho^+ = \delta_B(f) - f$; (d) proposed detail extraction operator i.e., $\overline{\psi}_\rho = 0.5(\rho^- - \rho^+) = 0.5(f - \epsilon_B(f)) + 0.5(f - \delta_B(f))$.

was implemented by the sequential application of opening and closing operators, $\psi_{\text{Toet}} = \phi_B\gamma_B$. The use of ψ_{Toet} in an undecimated approach was later suggested by the same authors for data fusion purposes [24]. In this case the decrease in resolution is obtained by considering SEs with progressively larger support across scales, leading to the operator: $T^l_{\text{Toet}} = \phi_{B_l}\gamma_{B_l}$.

In the works of Laporterie *et al.* [9,15], the decomposition filter was given by the semi-sum of opening and closing $\psi_{\text{TH}} = 0.5(\phi_B + \gamma_B)$. A justification for this choice is clear after some simple algebraic manipulations, showing that this operator is related to top-hats. Indeed the complementary operator $\overline{\psi}_{\text{TH}} = id - \psi_{\text{TH}}$, which has the purpose of extracting the details, can be written as

$$\overline{\psi}_{\text{TH}} = id - 0.5(\phi_B + \gamma_B) = 0.5[(id - \phi_B) + (id - \gamma_B)] \tag{6}$$

$$= 0.5(\text{WTH}_B - \text{BTH}_B) \tag{7}$$

It has also been reported in [21], that the difference between black and white top-hats is commonly used for enhancing the contrast of the images. The pyramidal scheme exploiting this filter was specifically proposed for pansharpening application in [13]. A downsampling is considered at each step for aliasing reduction, leading to the analysis operator $T^l_{\text{Lap}} = R^{\downarrow}\psi_{\text{TH}} = R^{\downarrow}0.5(\phi_B + \gamma_B)$.

An alternative way for obtaining a pyramidal decomposition is to extract high spatial frequency details by means of contrast operators. A notable example is the TC. Spatial details can be derived through the operator

$$\overline{\psi}_{\text{TC}} = \text{DTC}_B - \text{ETC}_B = \max(\text{TC}_B - id, 0) - \max(id - \text{TC}_B, 0), \tag{8}$$

defined in terms of Dilation and Erosion Toggle Contrast operators, DTC and ETC respectively [7]. In the context of data fusion TC has been used for multiscale representation through the application of the scale dependent filter

$\psi^l_{\mathrm{TC}} = id - \overline{\psi}^l_{\mathrm{TC}}$, without downsampling, namely $T^l_{\mathrm{TC}} = \psi^l_B$, where the superscript l indicates the size of the SE [7]. More recently, a decomposition operator combining the effects of both top-hats and toggle contrast operators was proposed by Bai *et al.* [6]: $T^l_{\mathrm{Bai}} = id - (\mathrm{WTH}_{B_l} - \mathrm{BTH}_{B_l}) - (\mathrm{DTC}_{B_l} - \mathrm{ETC}_{B_l})$.

In this work we propose to use *half-gradients* for performing the decomposition. The application of morphological gradients for enhancing the image contrast has been already evidenced [21]. However, to our knowledge, their application for data fusion tasks (e.g., pansharpening) is still unexplored. The effect of the internal and external gradients can be seen in Fig. 1(b,c), where the application to a piecewise-constant mono-dimensional signal f with a flat SE B with neighborhood $N_B = \{-1, 0, 1\}$ is shown. The results of the application of ρ^+ and ρ^- assume positive values in the presence of signal discontinuities. However, while the non zero values of the internal gradient follow the positive discontinuities and preceeds the negative ones, the opposite behavior is shown by the external gradient. Thus, the difference of the two operators reproduces the variations of the function with respect to the local mean, as reported in Fig. 1(d). Accordingly, we define the details extraction operator $\overline{\psi}_\rho$ as the difference of the two gradients

$$\overline{\psi}_\rho = 0.5(\rho^- - \rho^+) = 0.5(id - \epsilon_B) - 0.5(\delta_B - id),$$

in which the factor 0.5 is applied to preserve the dynamic range of the details. This is fundamental in pansharpening since otherwise, spatial artifacts would appear in the pansharpening product. Thus, the corresponding analysis filter is given by

$$\psi_\rho = id - \overline{\psi}_\rho = id - [0.5(id - \epsilon_B) - 0.5(\delta_B - id)] = 0.5(\epsilon_B + \delta_B), \qquad (9)$$

namely, the semi-sum of dilation and erosion. For the decomposition we apply the proposed operator in cascade with a dyadic subsampling, i.e., $T^l_\rho = R^{\downarrow} 0.5(\epsilon_B + \delta_B)$.

4 Numerical Results

Two data sets have been used to assess the performance of the proposed algorithm. As no High Resolution MS target image is available, the quantitative evaluation of pansharpening algorithm has been carried out with a reduced resolution assessment procedure [26].

4.1 Compared Algorithms

In this section we report the results of the proposed pansharpening method based on morphological multiscale analysis. Some features were fixed *a priori*. The number L of levels in the decomposition is set to $L = \log_2(r)$ with r the resolution ratio between the MS and the PAN image (typically $r = 4$ that implies $L = 2$). We choose the HPM injection scheme and employed a decimated/interpolated

decomposition exploiting dyadic subsampling and bilinear interpolation[1] in the analysis and synthesis phase, respectively. Thus the decomposition operator $T = 2^{\downarrow}\psi$ is fully specified by the choices of the analysis operator ψ and of the SE B, on which this work is focused. In the following we refer to the notation: MF-{*analysis operator*}-{*SE*} for referring to the analyzed algorithms. The four considered analysis operators are:

TH: Top-Hats [9,15]: $\psi_{\mathrm{TH}} = id - 0.5[(\mathrm{WTH}_B - \mathrm{BTH}_B)] = 0.5[\gamma_B + \phi_B]$;
TC: Toggle [21]: $\psi_{\mathrm{TC}} = id - 0.5[(\mathrm{DTC}_B - \mathrm{ETC}_B)]$;
BAI: Toggle+Top-Hats [6]: $\psi_{\mathrm{Bai}} = id - 0.5[(\mathrm{WTH}_B - \mathrm{BTH}_B) - (\mathrm{DTC}_B - \mathrm{ETC}_B)]$;
HGR: Half Gradients [Novel approach]: $\psi_\rho = id - 0.5(\rho^- - \rho^+) = 0.5[\epsilon_B + \delta_B]$.

Note explicitly that, in order to guarantee a fair comparison, a factor 0.5 was added to the detail extraction operator also for the methods proposed in [7] and [6].

Four different SEs were considered:

S: 3×3 squared SE
D: disk-shaped SE with radius 1
H: horizontal linear SE of length 3
V: vertical linear SE of length 3

In addition, test are also performed by considering a SE of size 1 (referred as **MF-1** in the results), which leads to the pyramidal scheme with identity analysis operator $\psi_1 = id$ that can be considered as a baseline for comparison since the decomposition is only based on the decimation step.

The proposed algorithms are also compared to several existing approaches, whose choice has been driven by the performances shown in public contests [5] or in the review [26]. Furthermore, we consider some data fusion strategies based on morphological pyramids. The following acronyms are used for the tested algorithms:

EXP: MS image interpolation (i.e., there is no injection of spatial details), using a polynomial kernel with 23 coefficients [2]
GIHS: *Fast Intensity-Hue-Saturation* (GIHS) image fusion [25]
SFIM: *Smoothing Filter-based Intensity Modulation* [16], based on *High-Pass Modulation* injection scheme and 5×5 box filter (*i.e.,* mean filter) for details extraction
MTF-GLP: *Generalized Laplacian Pyramid* (GLP) [2] with MTF-matched filter [3] with unitary injection model
AWLP: *Additive Wavelet Luminance Proportional* [19]

[1] The suitability of bilinear interpolation was already evidenced in [12] and confirmed in this study through the comparison with other interpolation schemes, based on zero-order, cubic, Lanczos-2 and Lanczos-3 kernels. The results are omitted for space constraints.

Table 1. Results obtained on the *Hobart 1* and *Rome data sets*. The comparison among different analysis operators ψ and SEs is reported with dyadic decomposition and bilinear interpolation for the expansion. Values of the Q^{2^n}, SAM, and $ERGAS$ are indicated. For each SE, the best results among operators are marked in bold while the second ones are underlined.

ψ	B	Q4	SAM	ERGAS	Q8	SAM	ERGAS
TH	S	**0.9035**	**4.8304**	3.0838	0.8914	3.9373	3.9785
	D	**0.9023**	4.8321	3.0144	0.8935	3.9691	3.7878
	H	0.8929	4.8416	3.1622	0.8863	4.0137	3.9377
	V	0.8935	4.8424	3.1548	0.8890	3.9956	3.8078
TC	S	0.8729	4.8615	3.3996	0.8731	4.0451	3.8722
	D	0.8731	4.8614	3.4014	0.8723	4.0576	3.9235
	H	0.8711	4.8651	3.4467	0.8705	4.0785	3.9659
	V	0.8707	4.8650	3.4483	0.8706	4.0753	3.9824
BAI	S	0.9020	4.8305	3.0841	0.8906	**3.9248**	3.9381
	D	**0.9023**	**4.8313**	2.9974	0.8951	3.9447	3.6673
	H	0.8936	4.8410	3.1449	0.8877	3.9946	3.8570
	V	0.8941	4.8412	3.1373	0.8905	3.9781	3.7352
HGR	S	0.8986	4.8382	**3.0073**	**0.8944**	3.9364	**3.4160**
	D	0.9011	4.8321	**2.9444**	**0.9014**	**3.8773**	**3.2884**
	H	**0.8960**	**4.8370**	**3.0491**	**0.8960**	**3.9367**	**3.4655**
	V	**0.8966**	**4.8377**	**3.0380**	**0.8982**	**3.8993**	**3.4144**
		Hobart 1 Dataset			*Rome Dataset*		

MF-Toet-HPF, approach proposed in [24]: $T^l_{\text{Toet}} = \phi_{B_l}\gamma_{B_l}$, B_l is a square of size $2l$ pixels, no decimation is done. The HPF injection scheme, or error pyramid, is used.

MF-Toet-HPM, approach proposed in [24]: $T^l_{\text{Toet}} = \phi_{B_l}\gamma_{B_l}$, B_l is a square of size $2l$ pixels, no decimation is done. The HPM injection scheme, or ratio pyramid, is used.

MF-Lap, approach proposed in [13,14,15]: $T_{\text{Lap}} = 2^{\downarrow}\psi_{\text{TH}}$, B is defined as a horizontal line of length two pixels and the expansion is done with a bilinear interpolation. The HPF injection scheme is used.

4.2 Experimental Results

In the reduced scale evaluation protocol [27] the low resolution data sets are simulated by degrading the spatial resolution of the available images by a factor $r = 4$. In greater details, the image scaling has been performed by applying a Gaussian-shaped low pass filter designed for matching the sensor's MTF [3]. In this case the original MS image acts as the *ground truth* (GT) and thus several indices can be used to assess the fused products. We employ here the *Spectral Angle Mapper* (*SAM)*, to evaluate the spectral quality of the images and two indexes accounting for both spatial and spectral quality: the $Q2^n$-index, and the *Erreur Relative Globale Adimensionnelle de Synthèse* (*ERGAS*). Please refer to [26] for details on these indexes. Optimal values are 0 for the SAM and the ERGAS and 1 for the $Q2^n$.

Table 2. Results on the *Hobart 1* and *Rome* data sets. Values of the Q^{2n}, and SAM and $ERGAS$ are reported. For each data set, the best result is marked in bold and the second best are underlined.

	Q4	SAM	ERGAS	Q8	SAM	ERGAS
EXP	0.6744	5.0314	5.1469	0.7248	4.9263	5.4171
GIHS	0.8256	4.9961	3.6727	0.7439	5.1455	4.1691
SFIM	0.8483	4.8961	3.6771	0.8758	4.2457	3.7591
AWLP	0.8910	5.0386	3.1703	0.9011	4.5146	3.3572
MTF-GLP	**0.9030**	**4.8263**	**2.9112**	**0.9016**	4.0957	3.2982
MF-1	0.8693	4.8666	3.4780	0.8684	4.0964	4.0899
MF-Toet-HPF	0.8743	4.9217	3.4821	0.8674	4.5915	4.1589
MF-Toet-HPM	0.8771	4.8739	3.5490	0.8606	4.4041	4.8072
MF-Lap	0.8827	4.8639	3.2440	0.8815	4.3085	3.7357
MF-HGR-S	0.8986	4.8382	3.0073	0.8944	3.9364	3.4160
MF-HGR-D	0.9011	4.8321	2.9444	0.9014	**3.8773**	**3.2884**
MF-HGR-H	0.8960	4.8370	3.0491	0.8960	3.9367	3.4655
MF-HGR-V	0.8966	4.8377	3.0380	0.8982	3.8993	3.4144
	Hobart 1 Dataset			Rome Dataset		

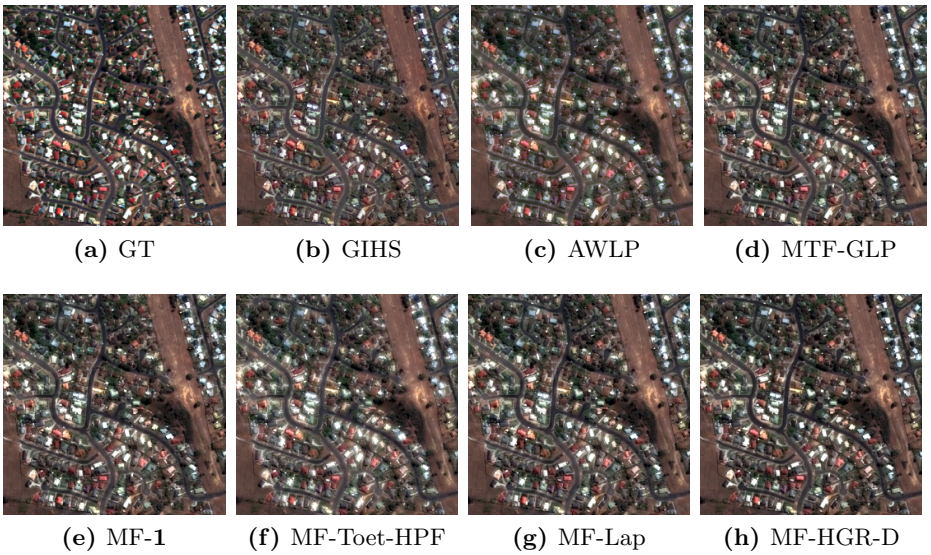

(a) GT **(b)** GIHS **(c)** AWLP **(d)** MTF-GLP

(e) MF-**1** **(f)** MF-Toet-HPF **(g)** MF-Lap **(h)** MF-HGR-D

Fig. 2. Results for the pansharpening algorithms on the *Hobart 1* data set: (a) GT; (b) GIHS; (c) MTF-GLP; (d) AWLP; (e) MF-**1**; (f) MF-Toet-HPF; (g) MF-Lap; (h) MF-HGR-D

Two data sets are employed for validation purposes. *Hobart 1* is a sample data set provided from GeoEye and referring to a scene of Hobart, Australia[2]. It is composed by a high resolution panchromatic channel and four MS bands. The

[2] Geoeye: Geoeye-1 Geo 8bit 0.5m True Color RGB - Hobart Aust 1, 02/05/2009 (2009).

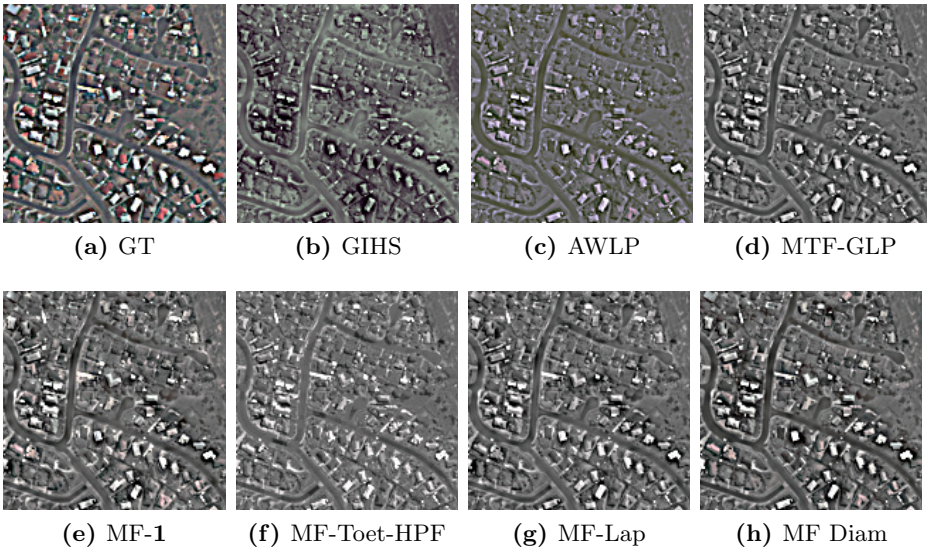

(a) GT **(b)** GIHS **(c)** AWLP **(d)** MTF-GLP

(e) MF-**1** **(f)** MF-Toet-HPF **(g)** MF-Lap **(h)** MF Diam

Fig. 3. Details injected by pansharpening algorithms on the *Hobart 1* data set: (a) GT; (b) GIHS; (c) MTF-GLP; (d) AWLP; (e) MF-**1**; (f) MF-Toet-HPF; (g) MF-Lap; (h) MF-HGR-D

images have a spatial resolution of 0.5 m and 2 m for PAN and MS, respectively. The dimension of the PAN image is 512×512 pixels. The *Rome* data set was instead acquired by the WorldView-2 sensor and represents the city of Rome, Italy. It is composed of a high resolution panchromatic channel and eight MS bands. The distributed images are characterized by a spatial resolution of 0.5 m and 2 m for PAN and MS, respectively. The dimension of the PAN image is 300×300 pixels.

The first analysis focuses on the comparison among the analysis operators and the SEs. The results achieved on the Hobart and Rome data sets, using a reduced resolution assessment, are reported in Table 1. A strong dependence of the obtained quality indexes on the ψ is straightforward. The decomposition scheme based on the HGR operator often shows the best performance, thus motivating the novel proposed approach.

A further comparison among the MF algorithms and several classical pansharpening approaches is proposed in Table 2. The first remarkable outcome is that the simplest implementation of the MF pyramidal schemes proposed in [24] and adjusted for the pansharpening applications in [13] yields fused products with low quality. Indeed, on both data sets the scheme proposed in this paper constitutes a significant enhancement with respect to the MF pansharpening literature and it confirms, even for this particular application, the remarkable capability of MFs in preserving the original features of the processed images.

Finally, a visual analysis is performed. We report in Fig. 2 the outcomes of the considered algorithms and the reference image (GT). The differences among the

presented methods are not easy to appreciate. Only the fusion method proposed in [24] reveals a very blurred image with an overall quality significantly worse than the other images. To ease the visual inspection only the injected details, i.e. the differences between the fused image $\widehat{\mathbf{MS}}$ and the original MS image upsampled at the PAN scale $\widetilde{\mathbf{MS}}$, are shown in Fig. 3. In this case the superior performances obtained by the proposed method are much more evident, both in terms of spectral and spatial accuracy.

5 Conclusions

Morphological filters have proven to be useful in several fields of image processing, as, for example, in segmentation and denoising applications. Nevertheless, their application in other research fields such as pansharpening, is rare. In this paper, we have focused our attention on exploring the capabilities of morphological filters in pansharpening. A reduced resolution quality assessment procedure has been performed on two real data sets acquired by the WorldView-2 and the GeoEye sensors. A comparison among morphological-based pyramid schemes using different operators and structuring elements has been carried out. Experiments have shown the validity of the proposed morphological pyramid scheme based on half gradients with respect to several state-of-the-art approaches.

References

1. Addesso, P., Conte, R., Longo, M., Restaino, R., Vivone, G.: A pansharpening algorithm based on genetic optimization of morphological filters. In: Proc. IEEE IGARSS, pp. 5438–5441 (2012)
2. Aiazzi, B., Alparone, L., Baronti, S., Garzelli, A.: Context-driven fusion of high spatial and spectral resolution images based on oversampled multiresolution analysis. IEEE Trans. Geosci. Remote Sens. 40(10), 2300–2312 (2002)
3. Aiazzi, B., Alparone, L., Baronti, S., Garzelli, A., Selva, M.: MTF-tailored multiscale fusion of high-resolution MS and Pan imagery. Photogramm. Eng. Remote Sens. 72(5), 591–596 (2006)
4. Aiazzi, B., Alparone, L., Baronti, S., Garzelli, A., Selva, M.: Advantages of Laplacian pyramids over "à trous" wavelet transforms. In: Bruzzone, L. (ed.) Proc. SPIE Image Signal Process. Remote Sens. XVIII. vol. 8537, pp. 853704–1–853704–10 (2012)
5. Alparone, L., Wald, L., Chanussot, J., Thomas, C., Gamba, P., Bruce, L.M.: Comparison of pansharpening algorithms: Outcome of the 2006 GRS-S data fusion contest. IEEE Trans. Geosci. Remote Sens. 45(10), 3012–3021 (2007)
6. Bai, X.: Morphological image fusion using the extracted image regions and details based on multi-scale top-hat transform and toggle contrast operator. Digit. Signal Process. 23(2), 542–554 (2013)
7. Bai, X., Zhou, F., Xue, B.: Edge preserved image fusion based on multiscale toggle contrast operator. Image and Vision Computing 29(12), 829–839 (2011)
8. Chavez Jr., P.S., Sides, S.C., Anderson, J.A.: Comparison of three different methods to merge multiresolution and multispectral data: Landsat TM and SPOT panchromatic. Photogramm. Eng. Remote Sens. 57(3), 295–303 (1991)

9. Flouzat, G., Amram, O., Laporterie-Déjean, F., Cherchali, S.: Multiresolution analysis and reconstruction by amorphological pyramid in the remote sensing of terrestrial surfaces. Signal Process. 81(10), 2171–2185 (2001)
10. Goutsias, J., Heijmans, H.J.A.M.: Nonlinear multiresolution signal decomposition schemes. I. morphological pyramids. IEEE Trans. Image Process. 9(11), 1862–1876 (2000)
11. Goutsias, J., Heijmans, H.J.A.M.: Nonlinear multiresolution signal decomposition schemes. II. morphological wavelets. IEEE Trans. Image Process. 9(11), 1897–1913 (2000)
12. Laporterie, F.: Représentations hiérarchiques d'images avec des pyramides morphologiques. Application à l'analyse et à la fusion spatio-temporelle de données en observation de la Terre. Ph.D. thesis (2002)
13. Laporterie-Déjean, F., Amram, O., Flouzat, G., Pilicht, E., Gayt, M.: Data fusion thanks to an improved morphological pyramid approach: comparison loop on simulated images and application to SPOT 4 data. In: Proc. IEEE IGARSS, pp. 2117–2119 (2000)
14. Laporterie-Déjean, F., Flouzat, G., Amram, O.: Mathematical morphology multilevel analysis of trees patterns in savannas. In: Proc. IEEE IGARSS, pp. 1496–1498 (2001)
15. Laporterie-Déjean, F., Flouzat, G., Amram, O.: The morphological pyramid and its applications to remote sensing: Multiresolution data analysis and features extraction. Image Anal. Stereol. 21(1), 49–53 (2002)
16. Liu, J.G.: Smoothing filter based intensity modulation: A spectral preserve image fusion technique for improving spatial details. Int. J. Remote Sens. 21(18), 3461–3472 (2000)
17. Maragos, P.: Morphological filtering for image enhancement and feature detection. In: The Image and Video Processing Handbook, 2nd edn., pp. 135–156. Elsevier Academic Press (2005)
18. Mukhopadhyay, S., Chanda, B.: Fusion of 2D grayscale images using multiscale morphology. Pattern Recogn. 34(10), 1939–1949 (2001)
19. Otazu, X., González-Audícana, M., Fors, O., Núñez, J.: Introduction of sensor spectral response into image fusion methods. Application to wavelet-based methods. IEEE Trans. Geosci. Remote Sens. 43(10), 2376–2385 (2005)
20. Shah, V.P., Younan, N.H., King, R.L.: An efficient pan-sharpening method via a combined adaptive-PCA approach and contourlets. IEEE Trans. Geosci. Remote Sens. 46(5), 1323–1335 (2008)
21. Soille, P.: Morphological Image Analysis: Principles and Applications. Springer (2003)
22. Starck, J.-L., Murtagh, F., Fadili, J.M.: Sparse image and signal processing: wavelets, curvelets, morphological diversity. Cambridge University Press (2010)
23. Toet, A.: A morphological pyramidal image decomposition. Pattern Recognition Letters 9(4), 255–261 (1989)
24. Toet, A.: Hierarchical image fusion. Mach. Vision App. 3(1), 1–11 (1990)
25. Tu, T.-M., Su, S.-C., Shyu, H.-C., Huang, P.S.: A new look at IHS-like image fusion methods. Inform. Fusion 2(3), 177–186 (2001)
26. Vivone, G., Alparone, L., Chanussot, J., Dalla Mura, M., Garzelli, A., Licciardi, G., Restaino, R., Wald, L.: A critical comparison among pansharpening algorithms. IEEE Trans. Geosci. Remote Sens. 53(5), 2565–2586 (2015)
27. Wald, L., Ranchin, T., Mangolini, M.: Fusion of satellite images of different spatial resolutions: Assessing the quality of resulting images. Photogramm. Eng. Remote Sens. 63(6), 691–699 (1997)